Synthesis of nano-capsules via aqueous emulsion RCMP-PISA and encapsulation

Sarkar, Jit; Jackson, Alexander W.; van Herk, Alexander M.; Goto, Atsushi

2020

Sarkar, J., Jackson, A. W., van Herk, A. M. & Goto, A. (2020). Synthesis of nano-capsules via aqueous emulsion RCMP-PISA and encapsulation. Polymer Chemistry, 11(23), 3904-3912. doi:10.1039/D0PY00465K

https://hdl.handle.net/10356/144155

https://doi.org/10.1039/D0PY00465K

Journal Name

ARTICLE

Synthesis of Nano-capsules via Aqueous Emulsion RCMP-PISA and Encapsulation

Received 00th January 20xx,
Accepted 00th January 20xx

DOI: 10.1039/x0xx00000x

www.rsc.org/

Jit Sarkar,[a] Alexander W. Jackson,[b] Alexander M. van Herk,[b*] and Atsushi Goto[a*]

Biocompatible nano-capsules (polymer vesicles) were prepared by combining NaI-catalyzed living radical polymerization with aqueous emulsion PISA (polymerization induced self-assembly). Poly(ethylene glycol) methyl ether methacrylate (PEGMA) and methyl methacrylate (MMA) were used as hydrophilic and hydrophobic monomers, respectively. Spheres and vesicles were generated depending on the degrees of polymerization of the hydrophilic and hydrophobic segments in the block copolymers. The spheres and vesicles were crosslinked using a divinyl monomer (ethylene glycol dimethacrylate (EGDMA)) as a co-monomer of MMA in situ during the polymerization. The encapsulation ability of the obtained vesicle was studied using a hydrophilic dye, i.e., Rhodamine-B.

Introduction

Polymer vesicles are nano-capsules with cavity. The shell is a bilayer of an amphiphilic block copolymer with hydrophobic and hydrophilic segments. In water, both outer and inner surfaces of the shell are hydrophilic. The inside of the bilayer is hydrophobic. Therefore, the vesicles can encapsulate hydrophilic molecules in the cavity and hydrophobic molecules in the shell layer. Such nano-capsules are widely used as delivery vehicles in cosmetics[1] and in drug delivery.[2] Extensive researches are dedicated to develop bio-compatible nano-capsules with high solid contents in solution and high loading capacity of guest molecules.

Nano-capsules (vesicles) and other self-assembly structures such as nano-spheres (micelles) and nano-cylinders (worms) can be obtained via the self-assembly of pre-synthesized block copolymers[3, 4] or the in situ formation of self-assembly during the polymerization. The latter is known as polymerization induced self-assembly (PISA) technique.[5-29] Reviews on PISA are available.[10-29] PISA is advantageous over the post assembly method, as PISA enables high solid contents (10-50% w/w) in solution because of the high colloidal stability.

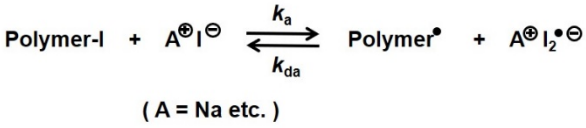

Scheme1. Reversible activation of RCMP.

In a previous work, we successfully combined NaI-catalyzed reversible complexation mediated polymerization (RCMP) with PISA for generating self-assemble structures, i.e., spherical micelles (spheres), worms, and vesicles, in ethanol with 5-9% solid contents.[30] The advantages of RCMP are no use of special capping agents, heavy metals, or sulfur compounds. RCMP uses a polymer-iodide (polymer–I) dormant species and a catalyst such as iodide anion (I^-).[31,32] Polymer–I and I^- are supposed to form a halogen-bonding complex (polymer–I···I^-). The complex subsequently reversibly generates the propagating radical (polymer$^\bullet$) and $I_2^{\bullet-}$ (Scheme 1). I^- is used in the form of salts such as NaI. Na is not a heavy metal. NaI is biologically safe, colourless, and odourless, suiting cosmetic and biological applications. In our previous work, we used block copolymers containing poly(methacrylic acid) (PMAA) as a hydrophilic segment and poly(methyl methacrylate) (PMMA) as a hydrophobic segment. Despite the successful generation of the self-assembly structures, an issue was the instability of the obtained self-assembly structures upon long-term storage due to the acid functionality of the hydrophilic segment (PMAA). The hydrogen bonding and electrostatic interaction between the acid groups caused the aggregation of the self-assembly structures and decreased their stability. Furthermore, PMMA is sensitive to skin and is not a bio-compatible segment. To address these issues, in the present work, we synthesized

[a] Division of Chemistry and Biological Chemistry, School of Physical and Mathematical Sciences, Nanyang Technological University, 21 Nanyang Link, 637371, Singapore.
[b] Institute of Chemical and Engineering Sciences, Agency for Science, Technology and Research, 1 Pesek Road, 627833, Singapore
Electronic Supplementary Information (ESI) available: Experimental Section. See DOI: 10.1039/x0xx00000x

stable nano-capsules with a bio-compatible segment, as described below. We also used water instead of ethanol as a solvent. Water is greener and the least expensive solvent, which is attractive in industrial applications.

PISA in water (aqueous PISA) has been conducted mainly via reversible addition-fragmentation chain transfer (RAFT) polymerization in the dispersion and emulsion systems. The monomer for the second block segment is fully miscible in water in the dispersion system and partially miscible in water in the emulsion system.[17] Because of the limited range of monomers amenable to the dispersion system, the emulsion system has been more extensively studied. Hawkett et al. reported a pioneering work of aqueous emulsion PISA, using acrylic acid and *n*-butyl acrylate.[5,33] Subsequently, Charleux et al. reported aqueous emulsion PISA with several hydrophilic monomers such as acidic,[34] basic,[35] and neutral monomers[36,37] and several hydrophobic monomers such as acrylates,[37] methacrylates,[36,38] and styrene[9] for generating spheres. Cunningham et al. reported the generation of spheres in aqueous emulsion PISA using benzyl methacrylate and a poly(glycerol monomethacrylate) macro-RAFT agent.[39] Armes et al. reported aqueous emulsion PISA for generating spheres,[40, 41] showing that the size of the sphere was dependent on the degree of polymerization (DP) of each segment. Perrier et al. reported the use of acrylates in aqueous emulsion PISA for generating spheres.[42] Assembly structures other than spheres were also prepared in aqueous emulsion PISA. Worms and vesicles were obtained by changing in the DPs of the segments and controlling the topology of the polymer.[43-46] A robust surfactant-free emulsion PISA was also utilized for producing vesicles with high (29%) solid content.[47] Armes et al. reported the generation of non-spherical monkey nut[48] and worm[49] morphologies. Monteiro et al. reported the synthesis of tadpoles.[50] D'Agosto, Rieger, and Charleux et al. reported nanofibers.[51,52] Tan et al. reported the use of a visible-light induced RAFT polymerization in aqueous emulsion PISA for obtaining spheres, worms, and vesicles.[53] Atom transfer radical polymerization (ATRP),[54,55] nitroxide mediated polymerization (NMP),[56-60] cobalt-mediated polymerization (CMP),[61,62] organotellurium-mediated radical polymerization (TERP),[63] and iodide-mediated polymerization[64] were also used for aqueous PISA.

The loading of guest molecules and guest nano-particles into the self-assemblies during PISA has extensively been studied for delivery and nano-reactor applications.[34,65-67] The guest molecules and particles were added to the PISA reaction solution and encapsulated in the self-assemblies in situ during PISA.

In the present paper, we report the use of RCMP in aqueous emulsion PISA to synthesize spheres and vesicles. We used poly(poly(ethylene glycol) methyl ether methacrylate) iodide (PPEGMA-I) as a hydrophilic macroinitiator in aqueous emulsion PISA of methyl methacrylate (MMA) as a hydrophobic monomer. We used water unlike our previous work using ethanol.[30] MMA is only partially miscible in water. Hence, the present system is an emulsion system, unlike the previously studied dispersion system using ethanol. PPEGMA is bio-compatible. In water, the obtained spheres and vesicles have a biocompatible PPEGMA segment on the surface of the shell, because PPEGMA is hydrophilic. The obtained assemblies may find applications in biomedical, food, and personal care use. The assembly structures depended on the DPs of hydrophilic and hydrophobic segments. We constructed the morphology diagram. The spheres and vesicles were also crosslinked using a divinyl monomer (ethylene glycol dimethacrylate (EGDMA)) as a co-monomer of MMA. We also studied the encapsulation of a hydrophilic guest molecule, i.e., Rhodamine-B (Rh-B) in vesicles (nano-capsules). Rh-B was selected because it is highly soluble in water and has strong UV-Vis absorption which facilitates quantification. We studied the loading efficiency.

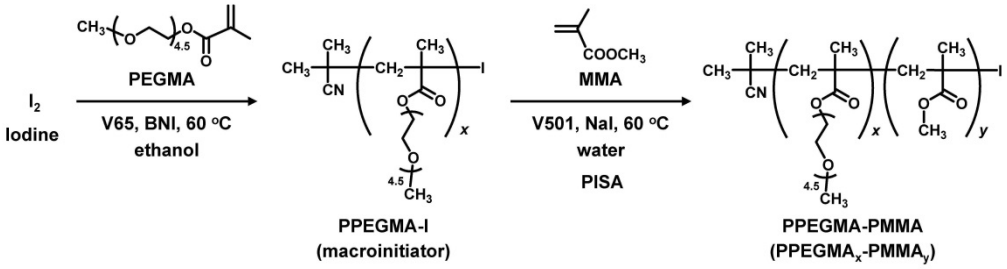

Scheme 2. Synthesis of PPEGMA-PMMA block copolymers.

Table 1. Synthesis of PPEGMA-I Macroinitiators.

entry	$[PEGMA]_0/[I_2]_0/[V65]_0/[BNI]_0$ (mM)[a]	T (°C)	t (h)	Conv.[b] (%)	M_n[c] ($M_{n,Theo}$[d])	DP[c]	$Đ$[c]
1	8000/40/160/80	60	3.5	75	27000 (22500)	90	1.31
2	8000/80/320/80	60	3.5	73	14000 (11000)	46	1.21
3	8000/160/640/80	60	4	70	9900 (5300)	33	1.16

[a] Solution polymerization in 20 wt% ethanol (solvent). [b] Monomer conversion was calculated from ^{1}H NMR analysis. [c] The M_n, DP, and $Đ$ values of PPEGMA-I were PMMA-calibrated GPC (DMF eluent) values after purification (reprecipitation). [d] Theoretical M_n value was calculated according to $([PEGMA]_0/(2[I_2]_0))\times$(monomer conversion)$\times$(molecular weight of PEGMA), assuming that one molecule of I_2 generates two molecules of R-I.

Results and discussion

Synthesis of PPEGMA-I Macroinitiator.

PPEGMA-I macroinitiators were prepared using RCMP (Scheme 2). We used poly(ethylene glycol) methyl ether methacrylate (PEGMA) as a monomer and tetrabutylammonium iodide ($Bu_4N^+I^-$) (BNI)[31] as a catalyst. We also used iodine (I_2) and 2,2-azobis(2,4-dimethylvaleronitrile) (V65) (an azo compound R-N=N-R) to in situ generate an alkyl iodide (R-I) dormant species during the polymerization. V65 generated the alkyl radical ($R^\bullet$) which reacted with I_2 to form R-I. The I_2/azo method was developed for iodide transfer polymerization (ITP) by Lacroix-Desmazes et al.[68] and subsequently utilized for RCMP.[31] We heated a mixture of PEGMA (average molecular weight = 300 g/mol) (200 equiv), I_2 (1 equiv), V65 (4 equiv), BNI (2 equiv), and ethanol (20 wt%, solvent) at 60 °C for 3.5 h (Table 1 (entry 1)). At 3.5 h, the monomer conversion reached 75%. The polymer was purified by reprecipitation using a mixture of hexane and diethyl ether (1:1 (v/v)) as a non-solvent. The number-average molecular weight (M_n (g/mol)) and dispersity ($Đ$) (= M_w/M_n) of the purified PPEGMA-I were 27000 and 1.31, respectively, where M_w is the weight-average molecular weight (g/mol). These values are not absolute values but PMMA-calibrated gel permeation chromatography (GPC) values. Therefore, the M_n value somewhat deviated from the theoretical M_n value (Table 1). As a rough estimate, we used the obtained M_n value to calculate the DP of the polymer to be 90. We use the estimated DP in the present paper. Similarly, we synthesized two other PPEGMA-I macroinitiators with the DPs of 46 and 33 (Table 1 (entries 2 and 3)). The three PPEGMA-I polymers were used as water-soluble macroinitiators in the emulsion RCMP-PISA of MMA in water (as shown below).

PISA.

$PPEGMA_{90}$-I (DP = 90) was used as a macroinitiator. In what follows, $PPEGMA_x$-$PMMA_y$ denotes a block copolymer with x DP of PPEGMA and y DP of PMMA. Previously, Zhu et al.[69] and Tan et al.[70] used PPEGMA macro-RAFT agent for aqueous emulsion PISA of MMA. We heated a mixture of MMA (400 equiv, monomer), $PPEGMA_{90}$-I (1 equiv, macroinitiator), 4,4-azobis(4-cyanovaleric acid) (V501) (2 equiv, azo initiator), NaI (8 equiv, catalyst), and water at 60 °C (Table 2 (entry 1)). V501 was used to increase the polymerization rate. Azo initiators are often used to decrease the deactivator concentration and hence effectively increase the polymerization rate in living radical polymerizations.[71,72] We studied a batch system containing the whole amount of monomer at the onset of polymerization. The solvent (water) was 90 wt%, and the total amount of the monomer and macroinitiator was 10 wt% (monomer/macroinitiator = 6/4). The solid content is 4% (macroinitiator) at a zero monomer conversion and will reach 10% at a full (100%) monomer conversion. The pH of the solution was adjusted to 7 by adding sodium bicarbonate ($NaHCO_3$). At pH = 7, V501 (azo initiator) containing acids was fully dissolved in water. Also, in an acidic or basic condition, the carbon-iodide bond at the polymer chain end tends to degrade to form a dead polymer chain. Therefore, the pH was adjusted to 7. The stirring speed was fixed to 1000 rpm in all studied cases, because lower speeds resulted in the coagulation of the assemblies in some cases.

After 4 h, the GPC chromatogram shows that a large fraction of the macroinitiator extended to block copolymers (Fig. 1a), indicating a high block-efficiency. A relatively high monomer conversion (83%) was attained at 4 h (Fig. 1b, Table 2 (entry 1)). The M_n value increased with an increase in the monomer conversion, and the $Đ$ value (1.27-1.50) was relatively low (Fig. 1c, Table 2 (entry 1)). The M_n values of the block copolymer (PPEGMA-PMMA) are PMMA-calibrated GPC values, resulting in the observed deviation of the experimental M_n value from the theoretical value (Fig. 1c). At 1.2 h, the PMMA segment (DP = 15) became long enough to be insoluble in water (Table 2 (entry 1)), and self-assemblies were generated. We obtained $PPEGMA_{90}$-$PMMA_y$ block copolymers with different y units (y = 15-480) between 1.2 h and 4 h. NaI (catalyst) would tend to be partitioned to the water phase more than the assembly phase. However, usually, the assembly phase is not fully hydrophobic but is more or less swollen with water. For this reason, NaI would still be able to be located in the assembly phase and catalyze the polymerization inside the assembly. The observed increase in the $Đ$ value at a later stage of polymerization would be ascribed to the generation of the additional chains from V501 (azo initiator) and the possible less partition of NaI in the assembly phase at a later stage of polymerization. At each sampling time, a small portion of the reaction mixture was taken out from the reactor and divided in three parts. The first part was dissolved in dimethylformamide (DMF) and subjected to GPC analysis. The second part was dissolved in deuterated dimethyl sulfoxide (DMSO-d_6) and subjected to ^{1}H NMR analysis to determine the monomer conversion. The third part was diluted by 50 times with water. This solution was used as the stock solution for the subsequent dynamic light scattering (DLS) and transmission electron microscope (TEM) studies.

We prepared TEM samples by casting a drop of the stock solution on a TEM grid, followed by drying in vacuum. Fig. 1d shows the TEM image of the self-assembly structure (vesicle) for $PPEGMA_{90}$-$PMMA_{480}$ obtained after the 4 h polymerization as an example. The self-assembly structure may change during the dilution and drying process in the preparation of TEM samples. However, the glass transition temperature of PMMA is approximately 100 °C, and thus the self-assembly structure would hardly change during the dilution and drying process at room temperature. More directly, as described below, the crosslinking experiments (in situ fixation of self-assembly structures during the polymerization) supported that the observed morphologies were really generated during the polymerization but not during the dilution or drying process.

The contour length of $PPEGMA_{90}$-$PMMA_{480}$ is 143 nm (= totally 570 units × 0.25 nm). The DLS measurement showed that the average diameter of the vesicles obtained with $PPEGMA_{90}$-$PMMA_{480}$ was 370 nm in a swollen state in water

(Table 2 (entry 1)). The diameter (370 nm) is larger than the twofold (286 nm) of the contour length (143 nm) of the copolymer. Therefore, the assembly structure was a vesicle but not a sphere. After 4 h, the solid content reached 9% (4% from the macroinitiator and 5% from the PMMA segment generated during the polymerization).

Morphology Diagram.

We constructed a morphology diagram using a series of hydrophilic PPEGMA-I macroinitiators with different DPs (33, 46, and 90) (Fig. 2). It should be noted that the boundaries of the morphologies are difficult to clearly define and should be viewed as a guide. The monomer/macroinitiator molar ratio in PISA was fixed to 400. We varied the DPs (from 16 to 480) of the hydrophobic PMMA segment with different monomer conversions (from 20% to 83%). We observed spheres and vesicles, depending on the DPs of the PPEGMA and PMMA segments. In the morphology diagram, the solid content was 4-9% (Figs. 2 and 3, Table 2).

In the PISA of MMA using $PPEGMA_{33}$-I (DP = 33 in the horizontal axis in Fig.2), the DP of PMMA segment (in the vertical axis in Fig. 2) increased from 21 to 91 with an increase in the polymerization time (Table 2 (entry 3)). The assembly structures were spheres for $PPEGMA_{33}$-$PMMA_{21}$ (with a small DP of PMMA) and changed to vesicles for $PPEGMA_{33}$-$PMMA_{91}$ (with a large DP of PMMA) through a mixed phase of spheres and vesicles for, e.g., $PPEGMA_{33}$-$PMMA_{61}$ (with a middle DP of PMMA), as observed in the TEM images (G, H, and I in Fig. 3). $PPEGMA_{33}$-$PMMA_{21}$ and $PPEGMA_{33}$-$PMMA_{31}$ were self-assembled to spheres. The diameters of the spheres determined in the DLS were 30 and 39 nm, respectively (Table 2 (entry 3)). The diameters were comparable with the twofold (26 and 32 nm, respectively) of the contour length of the block copolymers, which is consistent with the sphere structure. For $PPEGMA_{33}$-$PMMA_{91}$, the diameter (158 nm) of the obtained structure was larger than the twofold (62 nm) of the contour length of the block copolymer, which supports the vesicle structure. We did not observe worms in this study. Worms might be formed in a narrow composition range, or the system might not follow a typical PISA route. But, the TEM images confirmed that the larger structures are vesicles but not aggregation of spheres.

We also used two other macroinitiators $PPEGMA_{46}$-I and $PPEGMA_{90}$-I with higher DPs (Table 2 (entries 2 and 1, respectively)). Similar to $PPEGMA_{33}$-I, the structure changed from spheres to vesicles through the mixed phase with an increase in the DP of the PMMA segment for both macroinitiators (Figs. 2 and 3 (images A-F)). In principle, hydrophilic and hydrophobic mass fractions in the block copolymers determine the morphologies. The f_{PMMA} represents the mass (weight) fraction of the PMMA segment in the PPEGMA-PMMA block copolymer. In the present system, as a rough estimate, PPEGMA-PMMA forms spheres at $f_{PMMA} < 0.30$, a mixture of spheres and vesicles at $0.30 < f_{PMMA} < 0.46$, and vesicles at $f_{PMMA} > 0.46$. With an increase in the DP of the PMMA segment, the size of the assembly structure increased from 30-93 nm (spheres) to 158-370 nm (vesicles) in the studied cases (Table 2). Vesicles were obtained in water with 8-9% solid concentrations. The vesicles were tested for the encapsulation of guest molecules, as described below.

Table 2. Aqueous emulsion PISA of MMA with PPEGMA-I, NaI, and V501 in water at 60 °C (the weight ratios of water and a mixture of MMA and PPEGMA-I were 90% (water) and 10% (mixture of MMA and PPEGMA-I)).

Entry	DP of PPEGMA	$[MMA]_0/[PPEGMA\text{-}I]_0/[NaI]_0/[V501]_0$ (mM)[a]	t (h)	Conv. (%)	DP of PMMA[b]	$Đ$[b]	Symbol of Block Copolymer	f_{PMMA}	Hydrodynamic Diameter[c] in DLS (nm)	Size Distribution Index in DLS	Assembly Structure[d]	Code in Figs. 2 and 3
1	90	8000/20/160/40	1.2	20	15	1.27	$PPEGMA_{90}$-$PMMA_{15}$	0.05	35	0.243	S	
			1.8	28	25	1.27	$PPEGMA_{90}$-$PMMA_{25}$	0.08	45	0.203	S	A
			2.3	35	35	1.27	$PPEGMA_{90}$-$PMMA_{35}$	0.12	65	0.196	S	
			2.8	60	110	1.42	$PPEGMA_{90}$-$PMMA_{110}$	0.30	100	0.139	S+V	B
			4	83	480	1.50	$PPEGMA_{90}$-$PMMA_{480}$	0.64	370	0.590	V	C
2	46	8000/20/160/40	1	20	16	1.31	$PPEGMA_{46}$-$PMMA_{16}$	0.13	60	0.113	S	
			1.5	30	26	1.32	$PPEGMA_{46}$-$PMMA_{26}$	0.16	75	0.137	S	D
			2	35	34	1.31	$PPEGMA_{46}$-$PMMA_{34}$	0.20	85	0.143	S	
			2.5	41	42	1.32	$PPEGMA_{46}$-$PMMA_{42}$	0.23	93	0.127	S	
			3	54	58	1.28	$PPEGMA_{46}$-$PMMA_{58}$	0.30	100	0.210	S + V	
			3.5	66	78	1.26	$PPEGMA_{46}$-$PMMA_{78}$	0.36	135	0.329	S + V	E
			5	75	140	1.35	$PPEGMA_{46}$-$PMMA_{140}$	0.50	165	0.284	V	F
3	33	8000/20/160/40	1.2	35	21	1.17	$PPEGMA_{33}$-$PMMA_{21}$	0.18	30	0.124	S	
			1.8	43	31	1.21	$PPEGMA_{33}$-$PMMA_{31}$	0.24	39	0.134	S	G
			2.3	50	49	1.21	$PPEGMA_{33}$-$PMMA_{49}$	0.33	60	0.284	S	
			2.8	57	61	1.21	$PPEGMA_{33}$-$PMMA_{61}$	0.38	110	0.352	S + V	H
			3.8	67	91	1.24	$PPEGMA_{33}$-$PMMA_{91}$	0.48	158	0.366	V	I

[a] PPEGMA-I, NaI, and V501 were dissolved in water and subsequently mixed with MMA. [b] DP and $Đ$ values were determined with PMMA-calibrated DMF-GPC. [c] The DLS peak-top value. [d] S = sphere and V = vesicle.

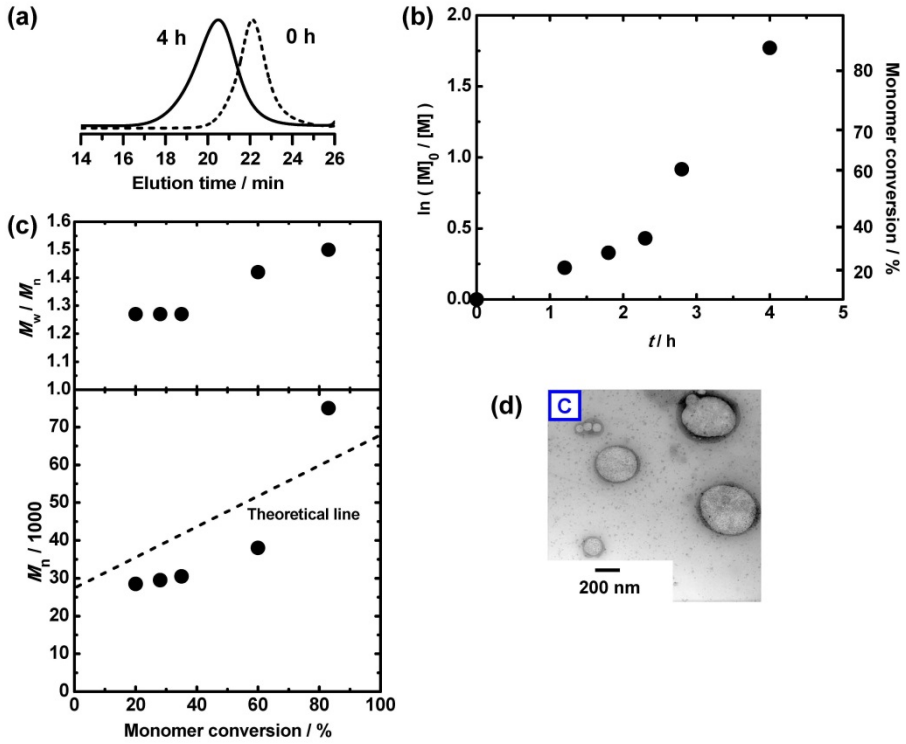

Fig. 1. (a) GPC chromatograms, (b) plot of $\ln([M]_0/[M])$ vs t, and (c) plots of M_n and M_w/M_n vs monomer conversion for the MMA/PPEGMA$_{90}$-I/NaI/V501/water system (60 °C): $[MMA]_0$ = 8 M; $[PPEGMA\text{-}I]_0$ = 20 mM; $[NaI]_0$ = 160 mM; $[V501]_0$ = 40 mM; water = 90 wt% (Table 2 (entry 1)). (d) TEM image of the vesicles generated at 4 h (the same TEM image as that in image C in Fig. 3).

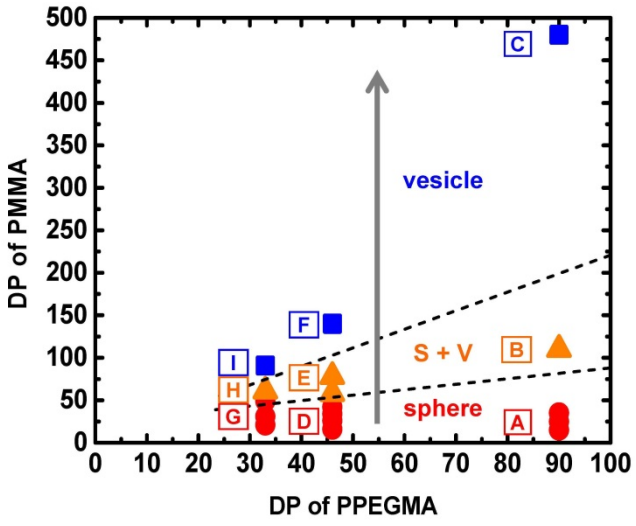

Fig. 2. Morphology diagram of the self-assembly structures generated in the aqueous emulsion PISA of PPEGMA-PMMA (Table 2). The solid content was 4-9 wt%. S + V denotes a mixture of spheres and vesicles.

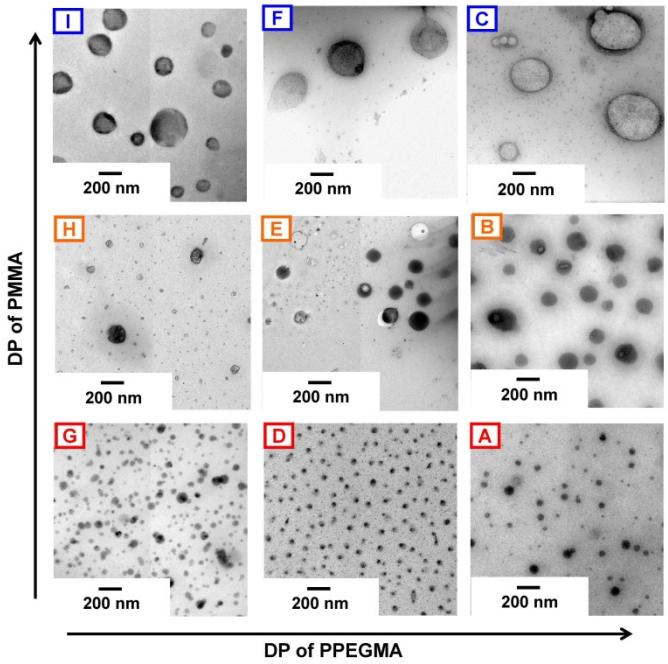

Fig. 3. TEM images of the self-assemblies obtained in the aqueous emulsion PISA process (Table 2 and Fig. 2), where A = PPEGMA$_{90}$-PMMA$_{25}$, B = PPEGMA$_{90}$-PMMA$_{110}$, C = PPEGMA$_{90}$-PMMA$_{480}$, D = PPEGMA$_{46}$-PMMA$_{26}$, E = PPEGMA$_{46}$-PMMA$_{78}$, F = PPEGMA$_{46}$-PMMA$_{140}$, G = PPEGMA$_{33}$-PMMA$_{31}$, H = PPEGMA$_{33}$-PMMA$_{61}$, and I = PPEGMA$_{33}$-PMMA$_{91}$.

Crosslinking.

In order to fix the assembly structures, a cross-linkable divinyl monomer, i.e., ethylene glycol dimethacrylate (EGDMA) was copolymerized with MMA in the PISA.

As mentioned above, $PPEGMA_{33}$-$PMMA_{31}$ (Fig. 3 (image G) and Table 2 (entry 3)) generated spheres and $PPEGMA_{33}$-$PMMA_{91}$ (Fig. 3 (image I) and Table 2 (entry 3)) generated vesicles. These non-crosslinked assemblies decomposed by the addition of tetrahydrofuran (THF), because both of the PPEGMA and PMMA segments are soluble in THF. DLS curves (Fig. 4, where the y-axis is the intensity) show that spheres (39 nm) and vesicles (158 nm) decomposed to single linear block copolymers (1.5 and 3.5 nm, respectively).

We replaced pure MMA with a mixture of MMA and EGDMA (Table 3) in these two PISA experiments ($PPEGMA_{33}$-$PMMA_{31}$ (spheres) and $PPEGMA_{33}$-$PMMA_{91}$ (vesicles)). We used a small amount of EGDMA (5 mol% for fixing the spheres and 3.8 mol% for fixing the vesicles) to prevent the crosslinking at an early stage of polymerization. Therefore, the crosslinking occurred only after the formation of assembly structures. We obtained similar structures, i.e., spheres for $PPEGMA_{33}$-$(PMMA/PEGDMA)_{31}$ (Fig. 5 (image J)) and vesicles for $PPEGMA_{33}$-$(PMMA/PEGDMA)_{91}$ (Fig. 5 (image K)). These assemblies were treated with THF. The spheres showed virtually no change in the DLS curves before and after the THF treatment (42 nm and 46 nm) (Fig. 5a, Table 3 (entry 1)), meaning that the spheres did not decompose. No change in the structure was also confirmed with the TEM image (Fig. 5 (image L)). For the vesicle, after treating with THF, the size slightly increased from 156 nm to 175 nm (Fig. 5b, Table 3 (entry 2)) probably because of the swelling of the shell in THF. The vesicle structures were maintained, as observed with TEM (Fig. 5 (image M)). Thus, the spheres and vesicles were successfully crosslinked. Importantly, the morphologies (spheres and vesicles) observed with TEM were the same with (Fig. 5 (images J and K)) and without (Fig. 3 (images G and I)) the crosslinking, confirming that the morphologies discussed above for the non-crosslinked systems were also truly generated during the polymerization but not generated during the TEM sample preparation.

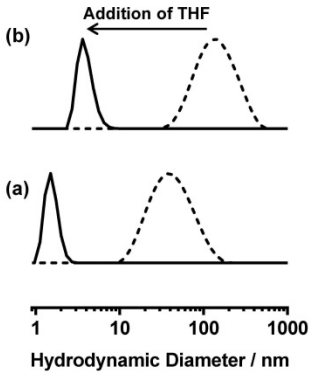

Fig. 4. DLS curves before (dashed lines) and after (solid lines) the addition of THF for (a) $PPEGMA_{33}$-$PMMA_{31}$ and (b) $PPEGMA_{33}$-$PMMA_{91}$ (Table 2 (entry 3)), where the y-axis is the intensity.

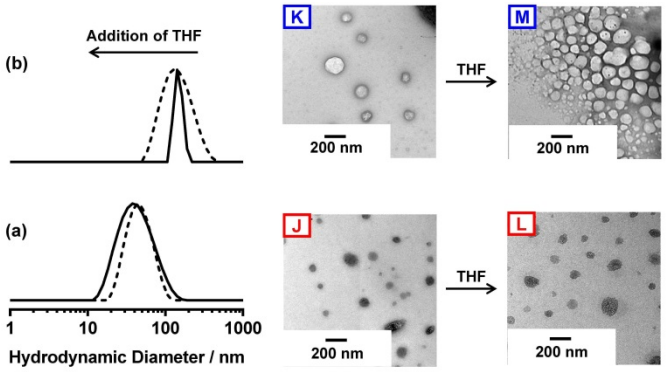

Fig. 5. DLS curves before (dashed lines) and after (solid lines) the addition of THF for (a) $PEGMA_{33}$-$(PMMA/PEGDMA)_{31}$ and (b) $PEGMA_{33}$-$(PMMA/PEGDMA)_{91}$ (Table 3), where the y-axis is the intensity. TEM images are those before and after the addition of THF for $PEGMA_{33}$-$(PMMA/PEGDMA)_{31}$ (images J and L) and $PEGMA_{33}$-$(PMMA/PEGDMA)_{91}$ (images K and M).

Encapsulation of Rhodamine-B in Nano-capsules.

The encapsulation of a guest molecule was studied using a vesicle prepared from $PPEGMA_{90}$-I macroinitiator. A hydrophilic dye Rh-B was used as a guest molecule. We performed the same polymerization as described in Table 2 (entry 1) in a non-crosslinked system except using an aqueous solution of Rh-B (15 mM in water) instead of pure water as a solvent. After 4 h, the monomer conversion reached 83% (Table 4). The DP of the PMMA segment was 450. The $Đ$ value (1.60) of the block copolymer obtained in the aqueous Rh-B solution was larger than that (1.50) obtained in pure water (Table 2 (entry 1 for 4 h)), showing that Rh-B slightly affected the polymerization.

After the polymerization, the reaction mixture was diluted with pure water (mixture/water = 1/10) and subsequently dialyzed in pure water for 84 h. Fig. 6 (image N) shows the vesicle after the dialysis. The core is dark, suggesting that Rh-B (dye) was loaded inside the core of the vesicle. Fig. 6 (image C) shows the vesicle obtained in pure water. The core is brighter than the shell, meaning that the core is empty. These results clearly demonstrate the successful loading of Rh-B. The DLS size of the vesicle was larger with Rh-B (476 nm) than without Rh-B (370 nm). Meanwhile, the vesicle structure (Fig. 6 (image N)) was maintained even after 84 h of dialysis. This result confirms that the vesicle structure was stable for a relatively long time (at least 84 h).

For quantitative discussion, we carried out a UV-Vis analysis of the aqueous solution of Rh-B-loaded vesicle (Fig. 7). We studied an aliquot before the dialysis and an aliquot after the dialysis. The former contained both encapsulated and unencapsulated Rh-B, and the latter contained only encapsulated Rh-B. We added acetone to these aliquots (aqueous solution/acetone = 1/4). The vesicles were decomposed with the addition of acetone and released Rh-B. The UV-Vis spectra of the acetone solutions (Fig. 7) showed the absorption of Rh-B with a peak top at 546 nm. The absorbance at the peak top before and after the dialysis was 1.751 (dashed line) and 0.348 (solid line), respectively. The

absorbance of 0.348 resulted from the Rh-B loaded in the vesicle (not from the solution). Thus, the encapsulation efficiency (fraction of the loaded Rh-B over the initially added Rh-B) was 20% (= 0.348/1.751). To confirm the complete removal of the unencapsulated Rh-B from the solution, the dialyzed solution was analyzed with UV-Vis spectroscopy. The UV-Vis spectrum (Fig. S1 in ESI) showed almost no absorbance, suggesting that the majority of the unencapsulated Rh-B was removed.

The average diameter of the Rh-B loaded vesicle in water was 476 nm, as determined by DLS (Table 4). We were not able to determine the shell thickness in water experimentally. The shell thickness in the dry state was approximately 33 nm from the TEM image. As a rough estimate, using this dry shell thickness (33 nm), we calculate the outer radius of the vesicle to be 238 nm (= 476/2 nm) and the inner radius of the vesicle to be 205 nm (= 238–33 nm) in water, giving a volume fraction of the cavity to be 64% (= $205^3/238^3$) and that of the polymer shell to be 36%. This calculation must be viewed as a rough estimate, because the shell thickness should be different in water and in the dry state. The total weight fraction of polymer in the solution was 9% (4% PPEGMA and 5% PMMA), as mentioned above. Assuming that the density of the shell is 1.18 g/cm^3 (density of bulk PMMA for the dry state (25 ^{o}C)) and that the density of the cavity is 1 g/cm^3 (water (25 ^{o}C)), the volume fraction of the vesicle in the solution is calculated to be 21% (= weight fraction of polymer in the solution (9%) / density of polymer (1.18 g/cm^3) / volume fraction of polymer in the vesicle (0.36)). The observed encapsulation efficiency (20%) is close to the calculated volume fraction of the vesicle in the solution (21%). This close accordance suggests that Rh-B was loaded not only in the core but also in the shell. The aromatic moiety of Rh-B may have affinity to the hydrophobic polymer shell, which may explain the loading in the shell. However, again, this calculation (21%) must be viewed as a rough estimate, while it gives some quantitative information for discussion. The loading capacity defined by the weight of the encapsulated Rh-B (0.009 g) divided by the weight of the polymer (7.5 g) was calculated to 0.12% in this particular study.

Table 3. Aqueous Emulsion PISA of MMA and EGDMA with $PPEGMA_{33}$-I, V501, and NaI (in 90 wt% Water) at 60 °C.

Entry	$[MMA]_0/[EGDMA]_0/[PPEGMA_{33}\text{-I}]_0/[V501]_0/[NaI]_0$ (mM)[a]	*t* (h)	Symbol of Block Copolymer[b]	Hydrodynamic Diameter in DLS (nm)[c]	Size Distribution Index in DLS	Assembly Structure[d]	Code in Fig. 5
1	7600/400/20/40/160	1.8	$PPEGMA_{33}$-$(PMMA/PEGDMA)_{31}$	42	0.199	S	J
	(after the addition of THF)			46	0.158	S	L
2	7700/300/20/40/160	3.8	$PPEGMA_{33}$-$(PMMA/PEGDMA)_{91}$	156	0.288	V	K
	(after the addition of THF)			175	0.840	V	M

[a] PPEGMA-I, NaI, and V501 were dissolved in water and subsequently mixed with MMA and EGDMA. [b] DP of (PMMA/PEGDMA) in entries 1 (1.8 h) and 2 (3.8 h) in Table 3 corresponds to DP of PMMA in entry 3 (1.8 h and 3.8 h) in Table 2. [c] The DLS peak-top value. [d] S = sphere and V = vesicle.

Table 4. Encapsulation of Rh-B in Vesicle Prepared in Aqueous Emulsion PISA of MMA with $PPEGMA_{90}$-I, V501, and NaI (in 90 wt% Water) at 60 °C.

$[MMA]_0/[PPEGMA_{90}\text{-I}]_0/[NaI]_0/[V501]_0$ (mM)[a]	*t* (h)	Conv. (%)	DP of PMMA[b]	*Đ*[b]	Hydrodynamic Diameter in DLS[c] (nm)	Size Distribution Index in DLS	Assembly Structure[d]	Dye in Capsules (encapsulation efficiency) (%)	Loading Capacity (%)
8000/20/160/40	4	83	450	1.60	476	0.821	V	20	0.12

[a] PPEGMA-I, NaI, Rh-B, and V501 were dissolved in water and subsequently mixed with MMA. The concentration of Rh-B in water was 15 mM. [b] DP and *Đ* values were determined with PMMA-calibrated DMF-GPC. [c] The DLS peak-top value. [d] V = vesicle.

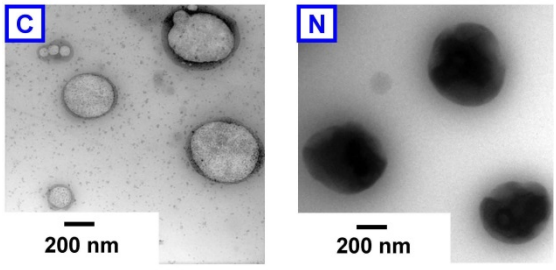

Fig. 6. TEM images of empty vesicles with $PEGMA_{90}$-$PMMA_{480}$ (image C) (Table 2 (entry 1)) and Rh-B-loaded vesicles with $PEGMA_{90}$-$PMMA_{450}$ (image N) (Table 4).

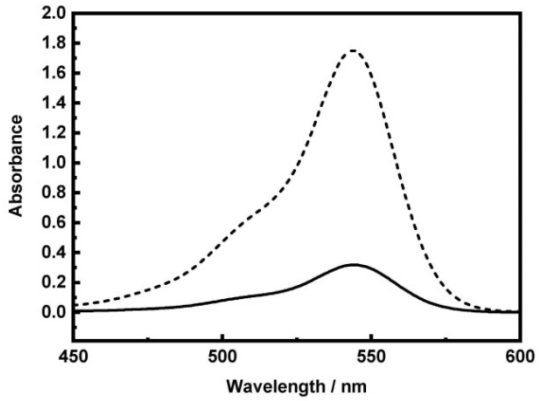

Fig. 7. Absorption spectra of the solutions of the Rh-B-loaded vesicle before (dashed line) and after (solid line) dialysis. The solution before the dialysis contained both encapsulated and unencapsulated Rh-B and that after the dialysis contained only encapsulated Ph-B.

Conclusions

Nano-particles (spheres) and nano-capsules (vesicles) were successfully prepared in aqueous emulsion RCMP-PISA of MMA using PPEGMA-I macroinitiators. Nano-capsules were generated when f_{PMMA} > 0.46. This system would suit biomedical, food, and personal care applications, because the PPEGMA segment located on the inner and outer surfaces of the shell is bio-compatible, the catalyst is non-toxic, and the solvent (water) is green and inexpensive. The nano-capsules were also crosslinked. Rh-B was successfully encapsulated at a 20% encapsulation efficiency and a 0.12% loading capacity, demonstrating the effective use of the obtained capsule as a container of a guest molecule.

Conflicts of interest

There are no conflicts to declare.

Acknowledgements

This work was partly supported by Advanced Manufacturing and Engineering Individual Research Grant (AME IRG) of Agency for Science, Technology and Research (A*STAR) (A1783c0001).

References

1. S. Nafisi and H. I. Maibach, in *Cosmetic Science and Technology*, eds. K. Sakamoto, R. Y. Lochhead, H. I. Maibach and Y. Yamashita, Elsevier, Amsterdam, 2017, 337-369.
2. R. Rajagopalan and J. V. Yakhmi, in *Nanostructures for Cancer Therapy*, eds. A. Ficai and A. M. Grumezescu, Elsevier, 2017, 211-240.
3. Y. Mai and A. Eisenberg, *Chem. Soc. Rev.*, 2012, **41**, 5969-5985.
4. E. Rideau, R. Dimova, P. Schwille, F. R. Wurm and K. Landfester, *Chem. Soc. Rev.*, 2018, **47**, 8572-8610.
5. C. J. Ferguson, R. J. Hughes, B. T. T. Pham, B. S. Hawkett, R. G. Gilbert, A. K. Serelis and C. H. Such, *Macromolecules*, 2002, **35**, 9243-9245.
6. E. Sprong, J. S. K. Leswin, D. J. Lamb, C. J. Ferguson, B. S. Hawkett, B. T. T. Pham, D. Nguyen, C. H. Such, A. K. Serelis and R. G. Gilbert, *Macromol. Symp.*, 2005, **231**, 84-93.
7. J. S. K. Leswin, J. Meuldijk, R. G. Gilbert and A. M. van Herk, *Macromol. Symp.*, 2009, **275–276**, 24-34.
8. Y. Li and S. P. Armes, *Angew. Chem., Int. Ed.*, 2010, **49**, 4042-4046.
9. X. Zhang, S. Boissé, W. Zhang, P. Beaunier, F. D'Agosto, J. Rieger and B. Charleux, *Macromolecules*, 2011, **44**, 4149-4158.
10. M. J. Monteiro and M. F. Cunningham, *Macromolecules*, 2012, **45**, 4939-4957.
11. N. J. Warren and S. P. Armes, *J. Am. Chem. Soc.*, 2014, **136**, 10174-10185.
12. J. Rieger, *Macromol. Rapid Commun.*, 2015, **36**, 1458-1471.
13. P. B. Zetterlund, S. C. Thickett, S. Perrier, E. Bourgeat-Lami and M. Lansalot, *Chem. Rev.*, 2015, **115**, 9745-9800.
14. M. J. Derry, L. A. Fielding and S. P. Armes, *Prog. Polym. Sci.*, 2016, **52**, 1-18.
15. Y. Zhu, B. Yang, S. Chen and J. Du, *Prog. Polym. Sci.*, 2017, **64**, 1-22.
16. A. B. Lowe, *Polymer*, 2016, **106**, 161-181.
17. S. L. Canning, G. N. Smith and S. P. Armes, *Macromolecules*, 2016, **49**, 1985-2001.
18. B. Charleux, G. Delaittre, J. Rieger and F. D'Agosto, *Macromolecules*, 2012, **45**, 6753-6765.
19. J.-T. Sun, C.-Y. Hong and C.-Y. Pan, *Polym. Chem.*, 2013, **4**, 873-881.
20. Q. Zhang and S. Zhu, *ACS Macro Letters*, 2015, **4**, 755-758.
21. S. Chen, P.-f. Shi and W. Zhang, *Chin. J. Polym. Sci.*, 2017, **35**, 455-479..
22. G. Cheng and J. Pérez-Mercader, *Macromol. Rapid Commun.*, 2019, **40**, 1970006.
23. S. Y. Khor, J. F. Quinn, M. R. Whittaker, N. P. Truong and T. P. Davis, *Macromol. Rapid Commun.*, 2019, **40**, 1800438.
24. X. Wang and Z. An, *Macromol. Rapid Commun.*, 2019, **40**, 1800325.
25. N. J. W. Penfold, J. Yeow, C. Boyer and S. P. Armes, *ACS Macro Lett.*, 2019, **8**, 1029-1054.
26. W.-J. Zhang, C.-Y. Hong and C.-Y. Pan, *Macromol. Rapid Commun.*, 2019, **40**, 1800279.
27. J. Yeow and C. Boyer, *Adv. Sci.*, 2017, **4**, 1700137.
28. J. Zhou, H. Yao and J. Ma, *Polym. Chem.*, 2018, **9**, 2532-2561.
29. F. D'Agosto, J. Rieger and M. Lansalot, *Angew. Chem., Int. Ed.*, 2020, **59**, 2-27.
30. J. Sarkar, L. Xiao, A. W. Jackson, A. M. van Herk and A. Goto, *Polym. Chem.*, 2018, **9**, 4900-4907.
31. A. Goto, A. Ohtsuki, H. Ohfuji, M. Tanishima and H. Kaji, *J. Am. Chem. Soc.*, 2013, **135**, 11131-11139.
32. J. Sarkar, L. Xiao and A. Goto, *Macromolecules*, 2016, **49**, 5033-5042.
33. C. J. Ferguson, R. J. Hughes, D. Nguyen, B. T. T. Pham, R. G. Gilbert, A. K. Serelis, C. H. Such and B. S. Hawkett, *Macromolecules*, 2005, **38**, 2191-2204.
34. I. Chaduc, A. Crepet, O. Boyron, B. Charleux, F. D'Agosto and M. Lansalot, *Macromolecules*, 2013, **46**, 6013-6023.
35. M. Manguian, M. Save and B. Charleux, *Macromol. Rapid Commun.*, 2006, **27**, 399-404.
36. J. Rieger, G. Osterwinter, C. Bui, F. Stoffelbach and B. Charleux, *Macromolecules*, 2009, **42**, 5518-5525.
37. J. Rieger, W. Zhang, F. Stoffelbach and B. Charleux, *Macromolecules*, 2010, **43**, 6302-6310.
38. X. Zhang, J. Rieger and B. Charleux, *Polym. Chem.*, 2012, **3**, 1502-1509.
39. V. J. Cunningham, A. M. Alswieleh, K. L. Thompson, M. Williams, G. J. Leggett, S. P. Armes and O. M. Musa, *Macromolecules*, 2014, **47**, 5613-5623.
40. S. L. Canning, V. J. Cunningham, L. P. D. Ratcliffe and S. P. Armes, *Polym. Chem.*, 2017, **8**, 4811-4821.
41. F. L. Hatton, J. R. Lovett and S. P. Armes, *Polym. Chem.*, 2017, **8**, 4856-4868.
42. P. Gurnani, C. Sanchez-Cano, K. Abraham, H. Xandri-Monje, A. B. Cook, M. Hartlieb, F. Lévi, R. Dallmann and S. Perrier, *Macromol. Biosci.*, 2018, **18**, 1800213.
43. S. Boissé, J. Rieger, K. Belal, A. Di-Cicco, P. Beaunier, M.-H. Li and B. Charleux, *Chem. Commun.*, 2010, **46**, 1950-1952.
44. S. Boissé, J. Rieger, G. Pembouong, P. Beaunier and B. Charleux, *J. Polym. Sci., Part A: Polym. Chem.*, 2011, **49**, 3346-3354.

45. J. Lesage de la Haye, X. Zhang, I. Chaduc, F. Brunel, M. Lansalot and F. D'Agosto, *Angew. Chem., Int. Ed.* 2016, **55**, 3739-3743.
46. I. Chaduc, E. Reynaud, L. Dumas, L. Albertin, F. D'Agosto and M. Lansalot, *Polymer*, 2016, **106**, 218-228.
47. 49. B. T. T. Pham, D. Nguyen, V. T. Huynh, E. H. Pan, B. Shirodkar-Robinson, M. Carey, A. K. Serelis, G. G. Warr, T. Davey, C. H. Such and B. S. Hawkett, *Langmuir*, 2018, **34**, 4255-4263.
48 A. A. Cockram, T. J. Neal, M. J. Derry, O. O. Mykhaylyk, N. S. J. Williams, M. W. Murray, S. N. Emmett and S. P. Armes, *Macromolecules*, 2017, **50**, 796-802.
49. F. L. Hatton, A. M. Park, Y. Zhang, G. D. Fuchs, C. K. Ober and S. P. Armes, *Polym. Chem.*, 2019, **10**, 194-200.
50. V. A. Bobrin and M. J. Monteiro, *J. Am. Chem. Soc.*, 2015, **137**, 15652-15655.
51. W. Zhang, F. D'Agosto, P.-Y. Dugas, J. Rieger and B. Charleux, *Polymer*, 2013, **54**, 2011-2019.
52. W. Zhang, F. D'Agosto, O. Boyron, J. Rieger and B. Charleux, *Macromolecules*, 2012, **45**, 4075-4084.
53. J. Tan, X. Dai, Y. Zhang, L. Yu, H. Sun and L. Zhang, *ACS Macro Lett.*, 2019, **8**, 205-212.
54. K. H. Kim, J. Kim and W. H. Jo, *Polymer*, 2005, **46**, 2836-2840.
55. X. Liu and W. Gao, *ACS Applied Materials & Interfaces*, 2017, **9**, 2023-2028.
56. S. Brusseau, F. D'Agosto, S. Magnet, L. Couvreur, C. Chamignon and B. Charleux, *Macromolecules*, 2011, **44**, 5590-5598.
57. X. G. Qiao, M. Lansalot, E. Bourgeat-Lami and B. Charleux, *Macromolecules*, 2013, **46**, 4285-4295.
58. G. Delaittre, J. Nicolas, C. Lefay, M. Save and B. Charleux, *Chem. Commun.*, 2005, **5**, 614-616.
59. G. Delaittre, C. Dire, J. Rieger, J.-L. Putaux and B. Charleux, *Chem. Commun.*, 2009, **20**, 2887-2889.
60. E. Groison, S. Brusseau, F. D'Agosto, S. Magnet, R. Inoubli, L. Couvreur and B. Charleux, *ACS Macro Lett.*, 2012, **1**, 47-51.
61. D. Cordella, A. Debuigne, C. Jérôme, Z. Kochovski, D. Taton and C. Detrembleur, *Macromol. Rapid Commun.*, 2016, **37**, 1181-1187.
62. D. Cordella, F. Ouhib, A. Aqil, T. Defize, C. Jérôme, A. Serghei, E. Drockenmuller, K. Aissou, D. Taton and C. Detrembleur, *ACS Macro Lett.*, 2017, **6**, 121-126.
63. Y. Kitayama, K. Kishida, H. Minami and M. Okubo, *J. Polym. Sci., Part A: Polym. Chem.*, 2012, **50**, 1991-1996.
64. Y. Ni, C. Tian, L. Zhang, Z. Cheng and X. Zhu, *ACS Macro Lett.*, 2019, **8**, 1419-1425.
65. B. Karagoz, L. Esser, H. T. Duong, J. S. Basuki, C. Boyer and T. P. Davis, *Polym. Chem.*, 2014, **5**, 350-355.
66. J. Yeow, S. Shanmugam, N. Corrigan, R. P. Kuchel, J. Xu and C. Boyer, *Macromolecules*, 2016, **49**, 7277-7285.
67. B. Karagoz, C. Boyer and T. P. Davis, *Macromol. Rapid Commun.*, 2014, **35**, 417-421.
68. P. Lacroix-Desmazes, R. Severac and B. Boutevin, *Macromolecules*, 2005, **38**, 6299-6309.
69. J. Wu, C. Tian, L. Zhang, Z. Cheng and X. Zhu, *RSC Advances*, 2017, **7**, 6559-6564.
70. X. Dai, L. Yu, Y. Zhang, L. Zhang and J. Tan, *Macromolecules*, 2019, **52**, 7468-7476.
71. A. Goto and T. Fukuda, *Prog. Polym. Sci.*, 2004, **29**, 329-385.
72. H. Fischer, *Chem. Rev.*, 2001, **101**, 3581-3610.

Graphical Abstract

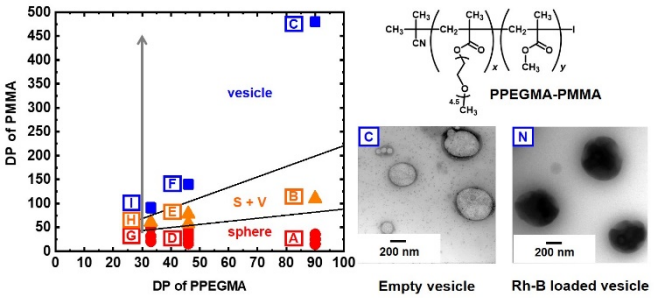

Synthesis of Nano-capsules Using Aqueous RCMP-PISA and Encapsulation of Rhodamine-B (Rh-B).